

# Termination of $\text{Ca}^{2+}$ Release for Clustered $\text{IP}_3\text{R}$ Channels

Sten Rüdiger<sup>1\*</sup>, Peter Jung<sup>2</sup>, Jian-Wei Shuai<sup>3\*</sup>

**1** Institut für Physik, Humboldt-Universität zu Berlin, Berlin, Germany, **2** Department of Physics and Astronomy, Ohio University, Athens, Ohio, United States of America, **3** Department of Physics and Institute of Theoretical Physics and Astrophysics, Xiamen University, Xiamen, China

## Abstract

In many cell types, release of calcium ions is controlled by inositol 1,4,5-trisphosphate ( $\text{IP}_3$ ) receptor channels. Elevations in  $\text{Ca}^{2+}$  concentration after intracellular release through  $\text{IP}_3$  receptors ( $\text{IP}_3\text{R}$ ) can either propagate in the form of waves spreading through the entire cell or produce spatially localized puffs. The appearance of waves and puffs is thought to implicate random initial openings of one or a few channels and subsequent activation of neighboring channels because of an “autocatalytic” feedback. It is much less clear, however, what determines the further time course of release, particularly since the lifetime is very different for waves (several seconds) and puffs (around 100 ms). Here we study the lifetime of  $\text{Ca}^{2+}$  signals and their dependence on residual  $\text{Ca}^{2+}$  microdomains. Our general idea is that  $\text{Ca}^{2+}$  microdomains are dynamical and mediate the effect of other physiological processes. Specifically, we focus on the mechanism by which  $\text{Ca}^{2+}$  binding proteins (buffers) alter the lifetime of  $\text{Ca}^{2+}$  signals. We use stochastic simulations of channel gating coupled to a coarse-grained description for the  $\text{Ca}^{2+}$  concentration. To describe the  $\text{Ca}^{2+}$  concentration in a phenomenological way, we here introduce a differential equation, which reflects the buffer characteristics by a few effective parameters. This non-stationary model for microdomains gives deep insight into the dynamical differences between puffs and waves. It provides a novel explanation for the different lifetimes of puffs and waves and suggests that puffs are terminated by  $\text{Ca}^{2+}$  inhibition while  $\text{IP}_3$  unbinding is responsible for termination of waves. Thus our analysis hints at an additional role of  $\text{IP}_3$  and shows how cells can make use of the full complexity in  $\text{IP}_3\text{R}$  gating behavior to achieve different signals.

**Citation:** Rüdiger S, Jung P, Shuai J-W (2012) Termination of  $\text{Ca}^{2+}$  Release for Clustered  $\text{IP}_3\text{R}$  Channels. *PLoS Comput Biol* 8(5): e1002485. doi:10.1371/journal.pcbi.1002485

**Editor:** Stanislav Shvartsman, Princeton University, United States of America

**Received:** August 26, 2011; **Accepted:** March 7, 2012; **Published:** May 31, 2012

**Copyright:** © 2012 Ruediger et al. This is an open-access article distributed under the terms of the Creative Commons Attribution License, which permits unrestricted use, distribution, and reproduction in any medium, provided the original author and source are credited.

**Funding:** This work was supported by the China National Funds for Distinguished Young Scientists under grant 11125419, the National Science Foundation of China under Grant 30970970 and National Institute of Health under grant 5R01GM065830 for Shuai. The funders had no role in study design, data collection and analysis, decision to publish, or preparation of the manuscript.

**Competing Interests:** The authors have declared that no competing interests exist.

\* E-mail: sten.ruediger@physik.hu-berlin.de (SR); jianweishuai@xmu.edu.cn (JWS)

## Introduction

$\text{Ca}^{2+}$  is a universal messenger of eukaryotic cells and regulates various cellular processes such as morphology, enzyme activity, and gene expression [1,2]. In many cells,  $\text{Ca}^{2+}$  signaling is achieved by modulation of cytosolic  $\text{Ca}^{2+}$  concentrations arising from exchange of  $\text{Ca}^{2+}$  with the endoplasmic reticulum (ER). SERCA pumps produce steep concentration gradients across the ER membrane by moving  $\text{Ca}^{2+}$  from the cytosol into the ER. Liberation of  $\text{Ca}^{2+}$  from the ER occurs through inositol 1,4,5-trisphosphate receptor ( $\text{IP}_3\text{R}$ ) channels in the ER membrane.

$\text{IP}_3\text{Rs}$  regulate  $\text{Ca}^{2+}$  transport in response to binding of  $\text{IP}_3$  and  $\text{Ca}^{2+}$  to receptor sites on the cytosolic domain of channels [3]. While binding of the second messenger  $\text{IP}_3$  generally promotes the opening of channels, the dependence on cytosolic  $[\text{Ca}^{2+}]$  is biphasic. Small increases in  $[\text{Ca}^{2+}]$  compared to rest level concentrations increase the open probability of  $\text{IP}_3\text{R}$  channels. The dissociation constant,  $K_{\text{act}}$ , of the responsible binding site is at sub- $\mu\text{M}$  scale. This stimulating  $\text{Ca}^{2+}$  binding gives rise to a self-amplifying mechanism called  $\text{Ca}^{2+}$  induced  $\text{Ca}^{2+}$  release (CICR):  $\text{Ca}^{2+}$  released by one or several channels diffuses in the cytosol and increases the open probability of neighboring channels by binding to their activating binding sites. As the level of  $\text{Ca}^{2+}$  rises further, inhibitory binding of  $\text{Ca}^{2+}$  dominates. Consequently, the open probability decreases significantly as  $\text{Ca}^{2+}$  levels reach values comparable to an inhibitory

dissociation constant,  $K_{\text{inh}}$ , at several tens of  $\mu\text{M}$ . Together, the activating and inhibiting binding processes allow for cooperative openings and closings of receptor channels.

Elevations of  $\text{Ca}^{2+}$  concentrations appear in two basic patterns that reflect the spatial organization of  $\text{IP}_3\text{R}$  channels [4]. In many cells,  $\text{IP}_3\text{R}$  channels are distributed in clusters on the ER membrane. It is often found that CICR synchronizes channels within clusters, resulting in patterns of localized and short-lived events called puffs [5]. In this regime,  $\text{Ca}^{2+}$  release does not spread to neighboring clusters, which are typically separated by a few  $\mu\text{m}$ . Recent studies emphasize the role of sub-cellular  $\text{Ca}^{2+}$  rises for physiological function [6–8].

In a different patterning mode, activity of channels from many clusters synchronizes to form cell-wide oscillations [9,10] or, in larger cells, waves [11]. Global release, lasting for up to several tens of seconds, is triggered by random initiation events (*i.e.*, random openings of a few channels) and carried through the cytosol by CICR between nearby clusters. It is important to note that waves do not only last longer because of the long time it takes to travel through the cell. After a wave has passed, elevations in  $[\text{Ca}^{2+}]$  persist for several seconds. In marked contrast, the calcium signal during a puff vanishes within around 100 ms [12]. This discrepancy and the related question how calcium signals are terminated provide the background for this publication.

Because of their spatial localization, puffs have been studied with theoretical methods by considering a single cluster and

## Author Summary

Calcium signals are important for a host of cellular processes such as neurotransmitter release, cell contraction and gene expression. While the principles of activation and spreading of calcium signals have been largely understood, it is much less clear how their spatio-temporal appearance is shaped. This issue is of high relevance since the spatio-temporal signature is thought to carry the information content. In our paper we study the dynamical mechanisms that determine the time course of calcium release from IP<sub>3</sub> receptor channels. We use a stochastic channel description combined with a recently developed model for the distribution of released calcium in a microdomain. The simulations uncover a complex control mechanism, which allows for the tuning of release from short frequent puffs to extended and less frequent wave-like release. Unexpectedly, the model predicts that for wave-like release the dissociation of IP<sub>3</sub> from the receptors leads to termination of the calcium signal. This effect relies on a well-known gating property of IP<sub>3</sub>R channels, which earlier has been regarded as superfluous in studies for groups of channels. Our results also provide a missing link to understand cellular Ca<sup>2+</sup> response to calcium-binding proteins and present a novel mechanism for information processing by IP<sub>3</sub>R channels.

ignoring the coupling to channels outside of the cluster. Recently, we and other groups have modeled puffs by a stochastic gating scheme for clustered channels coupled to evolution equations for local Ca<sup>2+</sup> concentration within the cluster microdomain [13–18]. The principal dynamics during a puff is sketched in the left panels of Fig. 1 and can be understood qualitatively by comparison of Ca<sup>2+</sup> levels with the dissociation constants  $K_{act,inh}$ . In an initial phase, random opening of a single channel in the cluster drives local [Ca<sup>2+</sup>] to values above the dissociation constant for activation:  $[Ca^{2+}] > K_{act}$  (dotted line). Fast intra-cluster CICR then causes further channels to open (left top panel, green line). Subsequently, Ca<sup>2+</sup> concentration within the cluster microdomain increases strongly. The local Ca<sup>2+</sup> concentration reaches values above the dissociation constant of inhibiting binding sites:  $[Ca^{2+}] > K_{inh}$  (left bottom panel, dashed line), which leads to inhibition (red line) and eventually to closing of channels.

Since the kinetic rates of the inhibitory sites of IP<sub>3</sub>Rs are large, the duration of puffs is short, matching the experimental observations [17]. Furthermore, the modeling predicts that subsequently channels loose Ca<sup>2+</sup> from the inhibition sites rapidly, usually within a time scale comparable to the puff duration. Thus the refractory time after a puff is normally small and channels are available for re-opening shortly after a puff ends [19].

Despite the impressive agreement of this modeling picture with experimental findings, the shortness of the refractory period raises an important question: If channels are inhibited only for tens or hundreds of milliseconds, calcium ions that have been released

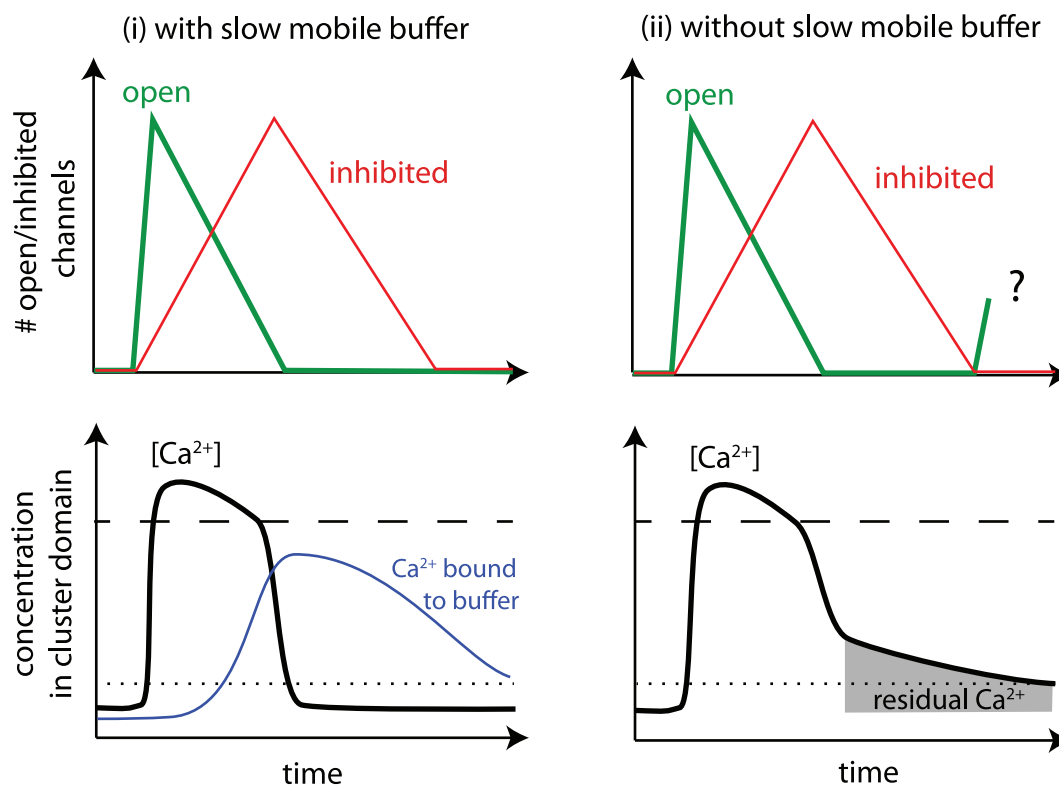


**Figure 1. Sketch of single cluster dynamics in presence of slow mobile buffer such as EGTA (i) and in its absence (ii).** Collective openings of channels (green lines, top panel) cause a rise in [Ca<sup>2+</sup>] (thick black lines) as well as subsequent slower inhibition of channels (red lines, top panel). Dotted and dashed lines in bottom panel provide comparison of Ca<sup>2+</sup> concentration with dissociation constants for activation,  $K_{act}$ , and inhibition,  $K_{inh}$ , respectively. Free Ca<sup>2+</sup> remains in the cluster microdomain transiently (right bottom panel), but its concentration can be reduced below  $K_{act}$  by buffer that binds residual Ca<sup>2+</sup> (blue line, left bottom panel). We here ask whether residual Ca<sup>2+</sup> leads to re-openings and, if so, what terminates release despite the re-openings.  
doi:10.1371/journal.pcbi.1002485.g001

during the previous puff could re-open the channels shortly by binding again to activating binding sites. The residual [Ca<sup>2+</sup>], caused by the Ca<sup>2+</sup> transiently remaining in the microdomain after the last open channel closes, could then be sufficiently large to re-open channels (Fig. 1, right panel). If such re-openings occur repeatedly over an extended period, release may last much longer than the experimentally measured duration of puffs. Using a standard model for IP<sub>3</sub> gating coupled to a simple law for [Ca<sup>2+</sup>] evolution, we first show in this paper that indeed large residual Ca<sup>2+</sup> microdomains can generate release at a long time-scale. Because the duration of those events reflects the temporal evolution in the wave regime, from here on we refer to this dynamical regime as waves.

The Ca<sup>2+</sup> microdomains and the dynamical evolution of residual [Ca<sup>2+</sup>] after channel closing was recently studied by us with numerical simulations of the detailed reaction-diffusion equations [20]. Importantly, we found that Ca<sup>2+</sup> levels can be decaying much slower than previously assumed. This result suggests that residual [Ca<sup>2+</sup>] and the mechanism we describe are relevant for the dynamics of Ca<sup>2+</sup> waves. This also implies that residual Ca<sup>2+</sup> could be a decisive factor for the observation of waves or puffs under different physiological conditions. In this paper we focus on the puff-wave transition under physiological changes related to Ca<sup>2+</sup> binding proteins.

It is well-known that Ca<sup>2+</sup> microdomains are very sensitive to certain mobile Ca<sup>2+</sup> binding and buffering proteins. The buffer proteins alter the distribution of Ca<sup>2+</sup> released from channels by reducing the spatial extent of microdomains [21]. Often this leads to strong effects on the dynamics of Ca<sup>2+</sup> release [12,21]. However, it was also found that a change of the microdomain extent is small for those buffers that bind Ca<sup>2+</sup> slowly. It therefore was a surprise that slow buffers such as EGTA and parvalbumin can dramatically change the appearance of Ca<sup>2+</sup> release. While for normal conditions, experiments under stimulating levels of IP<sub>3</sub> show a wave regime, in presence of slow buffers waves dissolve and puffs appear [12,22]. To explain this behavior we will here address a lesser known aspect of mobile buffers, which is that the temporal relaxation response of the microdomain (*i.e.*, the residual Ca<sup>2+</sup>) is affected.

Our simulations in [20] have shown that binding of Ca<sup>2+</sup> to slow buffers indeed lowers the amplitude of residual Ca<sup>2+</sup>. This effect can be substantial even though the effect on the Ca<sup>2+</sup> evolution during the puff is small (Fig. 1, left bottom panel). This

result suggests that the short duration of puffs, under buffered conditions, is caused by the fast decay of residual Ca<sup>2+</sup> concentrations. Here we therefore propose that the appearance of puffs in cells loaded with EGTA can be understood from the fact that residual Ca<sup>2+</sup> amplitudes are driven close to rest levels by binding to the buffer. Relating the action of buffer to a parameter of our [Ca<sup>2+</sup>] model, we show that indeed the modulation of Ca<sup>2+</sup> microdomain collapse can explain the puff-wave transition under control of buffer concentration.

This effect entails a final question that we would like to address here: If residual Ca<sup>2+</sup> causes sustained channel openings during waves, what then terminates the waves? While we find that puffs are terminated by Ca<sup>2+</sup> inhibition [13], we also find that the unbinding of IP<sub>3</sub> is responsible for termination of waves. Thus IP<sub>3</sub> plays a role not only in stimulation of Ca<sup>2+</sup> signals and in modulating their amplitude, but dynamics of IP<sub>3</sub> is also important for the termination of Ca<sup>2+</sup> waves. Taken together, this means that wave-like release requires binding of IP<sub>3</sub> to the receptor for stimulation, slow decay of residual Ca<sup>2+</sup> for sustaining the activity for several seconds, and finally unbinding of IP<sub>3</sub> for termination of the wave. Interestingly, the dynamical IP<sub>3</sub> binding/unbinding mechanism that we describe rests on the sensitivity of  $K_{inh}$  to IP<sub>3</sub> [3]. This sensitivity is a well-established property of the IP<sub>3</sub> gating to the receptor, but was hitherto neglected in theoretical and numerical studies of Ca<sup>2+</sup> release.

## Model

### Single channel gating

Equilibrium gating behavior of single channels has been investigated experimentally by patch-clamping [3,23]. Briefly, experimental results are the following: At small cytosolic Ca<sup>2+</sup> concentrations, an increase in [Ca<sup>2+</sup>] increases the probability of opening,  $P_o$ . For larger Ca<sup>2+</sup> concentrations, an increase in [Ca<sup>2+</sup>] leads to decreases in the open probability (Fig. 2A). Furthermore, binding of the second messenger IP<sub>3</sub> to the receptor increases the open probability. Fig. 2A shows that for higher levels of IP<sub>3</sub> the  $P_o$  curves are shifted upwards.

Several models have been proposed to discuss the open/close dynamics of a single IP<sub>3</sub>R channel [24,25]. Here we invoke the DeYoung-Keizer (DYK) model [24], which comprises the three basic binding processes of the receptor in its standard form. An IP<sub>3</sub>R consists of four identical subunits, each containing three

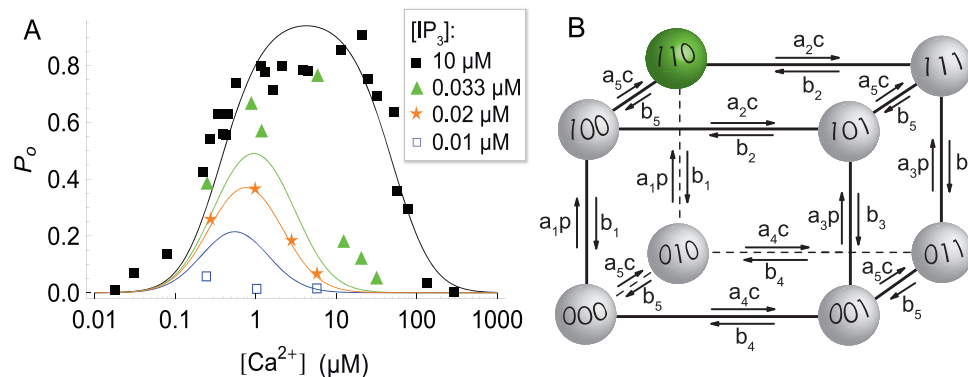


**Figure 2.** (A) Open probability for various values of cytosolic  $[Ca^{2+}]$  and IP<sub>3</sub> concentrations. Symbols are experimental results from [28,29], while lines are fitted using DeYoung-Keizer-type models. For increased IP<sub>3</sub> concentrations, curves shift upwards and the maximum shifts to the right. (B) DYK type models can be represented as transitions of each subunit along the edges of a cube. Rates of transitions involving binding of a molecule are proportional to the concentration of the respective molecule ( $p$  - IP<sub>3</sub> concentration,  $c$  - Ca<sup>2+</sup> concentration). The factors  $a_i$ ,  $b_i$  denote the on- and off-rates of binding of ligands to the respective sites. doi:10.1371/journal.pcbi.1002485.g002

binding sites: an activating site for Ca<sup>2+</sup>, an inhibiting Ca<sup>2+</sup> site, and an IP<sub>3</sub> binding site. The three binding sites allow for 8 different states for each subunit, which can be mapped onto triples (*ijk*) of each subunit. The index *i* indicates the state of the IP<sub>3</sub> site, *j* the one of the activating Ca<sup>2+</sup> site and *k* the state of the inhibiting Ca<sup>2+</sup> site. An index is 1 if a Ca<sup>2+</sup> ion or IP<sub>3</sub> is bound and 0 if not. Following earlier work we require at least three of the four subunits to be in the state (110) for the channel to open [26].

The 8 states allow for 24 different transitions, which can be associated with the edges of a cube (see Fig. 2B). Transitions between the respective subunit states are governed by rate constants, some of which are concentration dependent. There are five pairs of binding/unbinding rates, one for activation and two for inhibition and IP<sub>3</sub> binding, respectively. Each pair is given by the binding rate *a<sub>i</sub>* and the unbinding rate *b<sub>i</sub>*. The ratio, *d<sub>i</sub>* = *b<sub>i</sub>*/*a<sub>i</sub>*, is the dissociation constant, *d<sub>i</sub>*. In Fig. 2B, *c* denotes the Ca<sup>2+</sup> concentration and *p* denotes the IP<sub>3</sub> concentration in the cytosol.

We now discuss the properties of the IP<sub>3</sub>R channel model where we have fitted parameters *a<sub>i</sub>* and *b<sub>i</sub>* to experimental data (see Supporting Text S1). Solid lines in Fig. 2A show the open probability for a DYK model [27] where parameters were fitted against nuclear patch clamp data taken from [28,29].

The bell-like shape of the open probability curve is reflected in the different dissociation constants for activation (*d<sub>5</sub>*) and inhibition (*d<sub>2</sub>* and *d<sub>4</sub>*). Specifically, the open probability will be large for [Ca<sup>2+</sup>] above *d<sub>5</sub>* and below *d<sub>2,4</sub>*. Furthermore, in experiments the exact position of the peak open probability depends on the IP<sub>3</sub> concentration. Often, in the discussion of dynamical models, the IP<sub>3</sub> binding process is neglected, or it is absorbed into the activation and inhibition processes by assuming quasi-equilibrium.

The fact that for increasing IP<sub>3</sub> concentration the location of the right tail of the bell curve is sensitive to [IP<sub>3</sub>] is reflected in the DYK model by the existence of two dissociation constants for inhibition. Accordingly, *d<sub>2</sub>*, which is the dissociation constant for inhibition at large [IP<sub>3</sub>], should be much larger than *d<sub>4</sub>*, which is the dissociation constant at small [IP<sub>3</sub>]. Indeed, after fitting the DYK model we use *d<sub>2</sub>* = 78 μM while *d<sub>4</sub>* = 0.111 μM. In contrast, the activation threshold, quantified by *d<sub>5</sub>*, appears to remain constant (in our estimate at 0.25 μM, see Supporting Text S1).

Note that the IP<sub>3</sub> dependence of *d<sub>2</sub>* and *d<sub>4</sub>* also imposes a corresponding dependence of IP<sub>3</sub> affinity on the binding state of the inhibiting binding site. For all binding/unbinding loops given in Fig. 2B, the thermodynamic constraint requires that in equilibrium the dissociation constants satisfy the detailed balance conditions. Clearly, for a loop involving the activation process, the scheme shown in Fig. 2B is satisfying this condition. However, for a loop involving inhibition and IP<sub>3</sub> binding we obtain:

$$d_1 d_2 = d_3 d_4. \quad (1)$$

Thus it follows that the IP<sub>3</sub> dependence of inhibition requires *d<sub>1</sub>* ≠ *d<sub>3</sub>*, *i.e.*, the IP<sub>3</sub> binding depends on the inhibiting site. Because of *d<sub>2</sub>* ≫ *d<sub>4</sub>*, we then have *d<sub>3</sub>* ≫ *d<sub>1</sub>*. The fact that *d<sub>3</sub>* ≫ *d<sub>1</sub>* will play a crucial role in the interpretation of our results below.

### Clusters of IP<sub>3</sub>R channels and inhomogeneous Ca<sup>2+</sup> distribution

A major factor in the shaping of Ca<sup>2+</sup> signals is the clustered distribution of IP<sub>3</sub> channels on the membrane of the ER. Fluorescence visualization has shown that Ca<sup>2+</sup> is released through clusters of channels that comprise up to a few tens of channels. Early experimental studies showed that clusters occupy

domains of much less than one micrometer in diameter but could not resolve their inner structure. This led to a general model of a cluster as a small patch on the ER membrane, in which channels are distributed homogeneously and tightly packed. If channels in the cluster open, released calcium creates a *microdomain*, which is characterized by a large calcium concentration and, in this modeling picture, an approximately homogeneous distribution of calcium within the area. Subsequent progress in visualization, however, called this virtual domain picture into question [30] and prompted the inhomogeneous modeling which we will adapt in this study. A further strong hint on the inhomogeneous distribution of Ca<sup>2+</sup> within the cluster originated from our detailed comparison of stochastic simulations with experimental puff data from Smith and Parker [5]. If one assumes a homogeneous distribution of calcium within the cluster microdomain, as was often done in modeling approaches, the experimental amplitude distribution and lifetime of puffs cannot be fitted correctly. However, under the assumption of a non-homogeneous distribution of calcium, we were able to obtain a very accurate fitting of experimental data [17]. Here we further follow recent experimental results in assuming the typical peak open numbers to be 5–10 channels [31].

In our paper [20] we numerically simulated detailed models for IP<sub>3</sub>R clusters. Three-dimensional reaction-diffusion equations were used to calculate the evolution of [Ca<sup>2+</sup>] as well as that of relevant buffer proteins. These equations were coupled to a stochastic algorithm for the gating state of each channel. Ca<sup>2+</sup> influx through open channels was modeled by disk-shaped two-dimensional source areas on the surface of the simulation domain (see Fig. 3A). The radius of each channel's source area was set to 6 nm. The flux through the source area was adjusted to a current of 0.1 pA per channel in the open state. The size of the simulation domain was large enough (at the order of several μm) so that the released Ca<sup>2+</sup> does not significantly alter global Ca<sup>2+</sup> concentrations far away from the open channels. Channels were placed in regular lattices on the domain surface with distance on the order of several tens to hundreds of nm. A main result was that Ca<sup>2+</sup> is distributed very inhomogeneously in the cluster microdomain even for small distance of channels. While the concentration directly at the open pore is larger than 100 μM, we found much smaller concentrations in the space between channels, even if measured directly at the membrane surface between two open channels. We concluded that the influence that an open channel exerts to closed channels occurs at a much smaller Ca<sup>2+</sup> concentration than the feedback that the released Ca<sup>2+</sup> exerts to its own source channel (see Fig. 3B).

To reduce the complexity of this direct numerical approach we introduced a concept of scale separation. While the local concentration at the pore of open channels defines a relatively fixed and large value (denoted *c<sub>s</sub>* hereafter), the “coupling” concentration, *c<sub>d</sub>*, at any closed channel in the cluster is a much smaller quantity (Fig. 3B). In an approximation step we replaced this quantity by a suitable Ca<sup>2+</sup> average concentration for the microdomain [17,20], which is independent on the position of the closed and open channels within the cluster. Our simulations also showed that this quantity, which describes a typical concentration at closed channels within the microdomain, strongly depends on the number of open channels, *n*. Therefore, and taking into account a small rest level concentration *c<sub>0</sub>*, we obtain:

$$c_d(n) = c_0 + f(n), \quad (2)$$

where *f(n)* is a function of the number of open channels with *f(0)* = 0. This ansatz assumes that the [Ca<sup>2+</sup>] at any closed

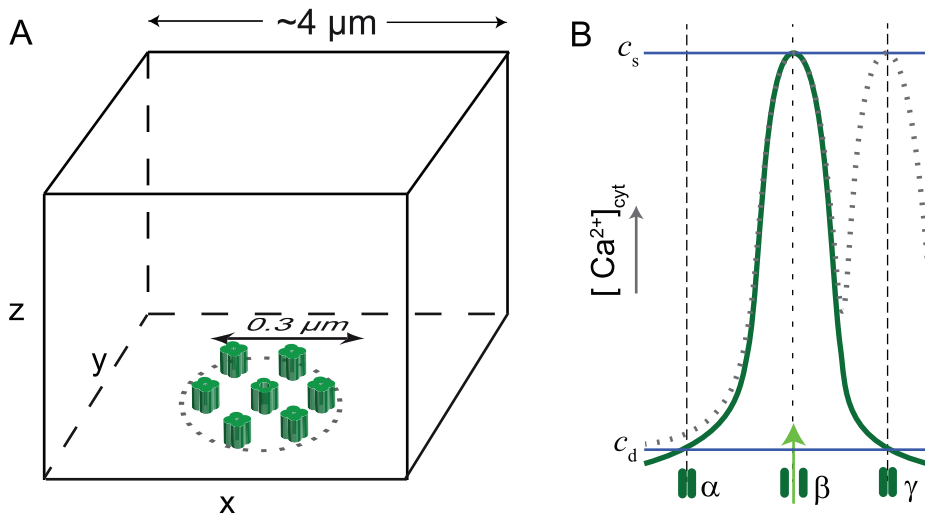


**Figure 3.** (A) Sketch of the basic setup of our model of IP<sub>3</sub>R clusters. Receptors are located on the ER membrane, which is represented by the bottom side of the box. The inside of the box, corresponding to cytosolic space, covers a domain of several  $\mu\text{m}$  in each dimension. It models the spatial domain around each cluster. This space provides the surrounding into which released Ca<sup>2+</sup> diffuses and does not contain any further Ca<sup>2+</sup> sources. The diameter of clusters is of the order of hundreds of nm (out of scale in the sketch). (B) Illustrates our understanding of Ca<sup>2+</sup> distribution after opening of channels. For simplification three channels located on a row are considered. Numerical simulations have shown that Ca<sup>2+</sup> is distributed very inhomogeneously within the cluster microdomain [20]. If a single channel is open (denoted by  $\beta$ ), release generates a three-dimensional distribution, which is locally peaked at the open channel and strongly decays away from the channel (blue curve). Thus there are two different scales of [Ca<sup>2+</sup>] as far as feedback of released Ca<sup>2+</sup> onto the channels is concerned: The first is large at hundreds of  $\mu\text{M}$  ( $c_s$  in the figure). It represents the feedback of the released Ca<sup>2+</sup> onto the open channel. Much smaller [Ca<sup>2+</sup>] occurs at the location of closed channels ( $c_d$  at order of  $10 \mu\text{M}$ ). If two or more channels are open, Ca<sup>2+</sup> levels increase as illustrated by the dotted line for open channels  $\beta$  and  $\gamma$ . For simplification,  $c_d$  is here taken to be independent on the distance of channels within the cluster. Description by  $c_{s,d}$  provides a powerful reduction of the complexity of Ca<sup>2+</sup> distribution. The approach can be likened to a coarse-graining but with keeping the feedback separated at two scales.  
doi:10.1371/journal.pcbi.1002485.g003

channel in the cluster follows the number of  $n$  open channels in a quasi-stationary way. In fact, earlier simulations have shown that local increases in the concentration quickly relax to a stationary profile after channel opening [20,32,33]. In this situation, the stationary approximation in Eq. 2 is justified. Below we will complement it with a simple description of temporal relaxation of  $c_d$  after channel closing.

We now summarize the static [Ca<sup>2+</sup>] part of the modeling features for IP<sub>3</sub>R clusters:

- Ca<sup>2+</sup> released from a channel creates a nanodomain near the channel pore, which is spatially small but exhibits Ca<sup>2+</sup> at very high concentration. An open channel is exposed directly to this nanodomain. Consequently, the Ca<sup>2+</sup> concentration governing further gating transitions of the open channel is large. We denote the corresponding concentration value by

$$c = c_s \quad (\text{local concentration at open channel, nanodomain}) \quad (3)$$

and choose  $c_s = 500 \mu\text{M}$  for our simulations [33].

- If a channel is closed, the local concentration at that channel originating from Ca<sup>2+</sup> released by  $n$  other open channels is described well by a linear relation [17]

$$c_d(n) = c_0 + c_1 n. \quad (4)$$

This quantity provides a typical concentration within the cluster microdomain. If channels are open ( $n > 0$ ),  $c_d$  is much larger than the Ca<sup>2+</sup> concentration a few  $\mu\text{m}$  away from the cluster. But it is also much smaller than the local value  $c_s$  at the pore of an open channel. In [17] we concluded from detailed

comparison with experimental results that the scale-separation is needed for agreement. We here use  $c_0 = 0.02 \mu\text{M}$  and  $c_1 = 4.0 \mu\text{M}$ , where  $c_0$  denotes the resting level concentration of Ca<sup>2+</sup>.

We will assume a cluster that consists of 20 channels. The values of  $c_{s,d}$  can be determined by two different methods. If one knows the full time-dependent evolution of the Ca<sup>2+</sup> distribution during puffs,  $c_s$  and  $c_d$  and their dependence on the number of open channels can be determined by averaging the local [Ca<sup>2+</sup>] at all open channels or all closed channels, respectively [17,20]. They can, however, also be introduced as phenomenological parameters. In [17] we have determined realistic values and have shown that this latter approach yields a very accurate description of experimentally observed puffs. The parameter value for the coupling concentration  $c_d$  corresponds to a cluster with radius of around 300 nm. As will be seen below, this setup leads to typical numbers of open channels of around 5–10, consistent with experiments in neuroblastoma cells.

### Non-stationary microdomains and mobile buffers

A further important factor in Ca<sup>2+</sup> signaling is the role of Ca<sup>2+</sup> buffers. It is well-known that mobile buffers can strongly reduce the size of microdomains and thereby also decrease the amount of Ca<sup>2+</sup> that reaches a target by diffusion. Here, however, we would like to focus on a property of buffers, which was much less studied so far, namely the influence of buffers on the microdomain collapse after channel closing, *i.e.*, the residual Ca<sup>2+</sup>.

In [20] we have studied the effect of mobile and immobile buffers on microdomains. By detailed numerical simulations of three-dimensional reaction-diffusion equations we characterized the alteration of open channel domains by buffers. Most

importantly, we found that mobile buffers reduce the amount of residual Ca<sup>2+</sup>. This happens because mobile buffers may bind free Ca<sup>2+</sup> and support the transport of Ca<sup>2+</sup> away from the microdomain. They, therefore, speed up the collapse of residual [Ca<sup>2+</sup>].

We also described in [20] which buffers can reduce the spatial extension of a domain around an open channel. It happens only if the buffer is mobile *and* has fast reaction kinetics. As described in [20] the fast mobile buffer plays a crucial role in reducing the coupling of channels within a cluster. Within our modeling approach this would result in a decrease of coupling constant  $c_1$  in Eq. 4 owing to the presence of fast mobile buffer. However, we are here interested in the role of slow mobile buffers, such as EGTA, which have little effect on the spatial extent of microdomain. Therefore, in the remainder of this paper, we neglect any changes of spatial appearance. We will therefore fix the coupling parameter  $c_1$  and exclusively study the effect of microdomain [Ca<sup>2+</sup>] decay caused by slow mobile buffers.

It remains to cast the temporal evolution law for the Ca<sup>2+</sup> microdomain after changes in the open channel number. As has been described earlier, after opening of a channel, the equilibration of [Ca<sup>2+</sup>] within the microdomain occurs very fast [20,32]. Therefore, we assume instantaneous [Ca<sup>2+</sup>] equilibration according to Eq. 4 after an increase in open channel number  $n$ . However, after channel closing, residual Ca<sup>2+</sup> remains and we here use an approximation of this microdomain collapse with an exponential equilibration:

$$\frac{dc}{dt} = r(c_d(n) - c) \quad (\text{closed channel in the microdomain}). \quad (5)$$

Here  $c_d(n)$  is given by Eq. 4.  $r$  is the rate of equilibration. Obviously, this simple law does not reflect the full complexities in the microdomain collapse but it does here serve as the most simple model for qualitative analysis [20,34].

### Summary of method

A summarizing chart of our model is given in Fig. 4. In the following we simulate clusters of 20 IP<sub>3</sub>R channels. Each subunit of each channel undergoes stochastic transitions according to the scheme shown in Fig. 2B. We use a standard stochastic algorithm based on a small time-step  $\tau$ . For each time step the algorithm determines for

each subunit whether a state transitions occurs (for a description of the stochastic simulation method see Supporting Text S2).

The channel is considered open if at least three of its four subunits are in the state 110, otherwise it is considered closed. The Ca<sup>2+</sup> concentration variable  $c$  appearing in the scheme in Fig. 2B is a quantity that follows the (stochastic) number of open channels in the cluster. It is governed by our coarse-grained deterministic model and  $c$  is thus not intrinsically stochastic. In each time step we determine the Ca<sup>2+</sup> concentration from the number of open channels  $n$  and by the two-scaled Ca<sup>2+</sup> concentrations given by Eqs. 3–5. More specifically, for all subunits that belong to closed channels,  $c$  is given by the value in differential equation 5. Subunits that belong to open channels will be given  $c = c_s$  in scheme Fig. 2B.

Finally, the value  $p$  in scheme Fig. 2B is the IP<sub>3</sub> concentration. Our choice of [IP<sub>3</sub>] will be within a range of concentrations where non-trivial dynamics can be expected. Recent experimental estimation of [IP<sub>3</sub>] during Ca<sup>2+</sup> release have shown that values of [IP<sub>3</sub>] between 50 and 100 nM are optimal for the appearance of Ca<sup>2+</sup> oscillations in COS-7 cells [35]. We will use values in the according range in the following discussions.

Parameters in the ordinary differential equation for  $c$  depend on the cellular physiology. For instance, the coupling constant  $c_d$  depends on the distance of channels and the presence of Ca<sup>2+</sup> buffers. However, in the current study we only consider changes in the relaxation rate  $r$ . An increase of  $r$  corresponds to a faster collapse of the Ca<sup>2+</sup> microdomain. Large  $r$  (here typically  $r = 100 \text{ s}^{-1}$ ) thus represents the case of EGTA-influenced release, while small  $r$  ( $r = 10 \text{ s}^{-1}$ ) represents the normal, unimpeded case.

## Results

### Dependence of release dynamics on [IP<sub>3</sub>]

A first analysis concerns the behavior of release events under changes of [IP<sub>3</sub>] using a decay rate of  $r = 10 \text{ s}^{-1}$ . This small value of  $r$  and the resulting slow temporal collapse of the Ca<sup>2+</sup> microdomain, can be viewed as a control “experiment” without slow mobile buffer. Fig. 5 shows the typical time evolution of the number of open channels and the microdomain concentration  $c$  for two different values of IP<sub>3</sub> concentration. In both cases, well-defined release events (puffs or wave-like bursts) are apparent.

To analyze their properties statistically, we now define a release event based on the evolution of the number of open channels. An

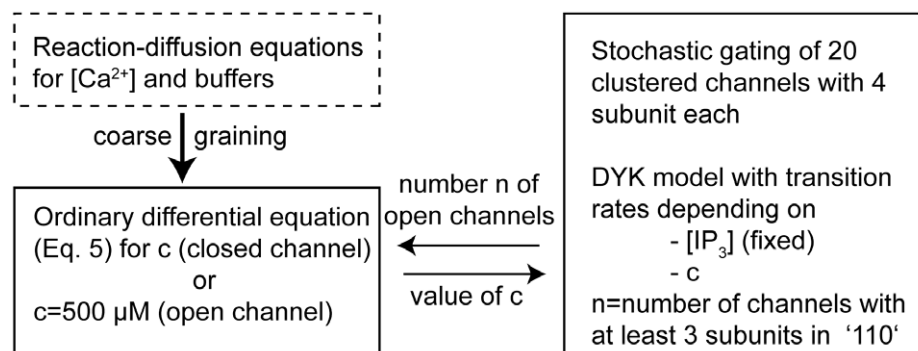


**Figure 4. Chart of the basic modeling setup used in this study.** A deterministic scheme for the Ca<sup>2+</sup> concentration is coupled to a stochastic description of channel gating (solid boxes). The state of 20 channels is simulated using a kinetic Monte-Carlo method. The number of open channels is determined at each instance of time. From the number of open channels one determines the concentration of Ca<sup>2+</sup> at open and closed channels using a fixed value or an ordinary differential equation, respectively. This reduced model is obtained by coarse-graining from direct numerical simulations of the full partial differential equations (dashed box). Parameters of the coarse-grained model depend on the physiological parameters such as channel distance and Ca<sup>2+</sup> buffers. doi:10.1371/journal.pcbi.1002485.g004

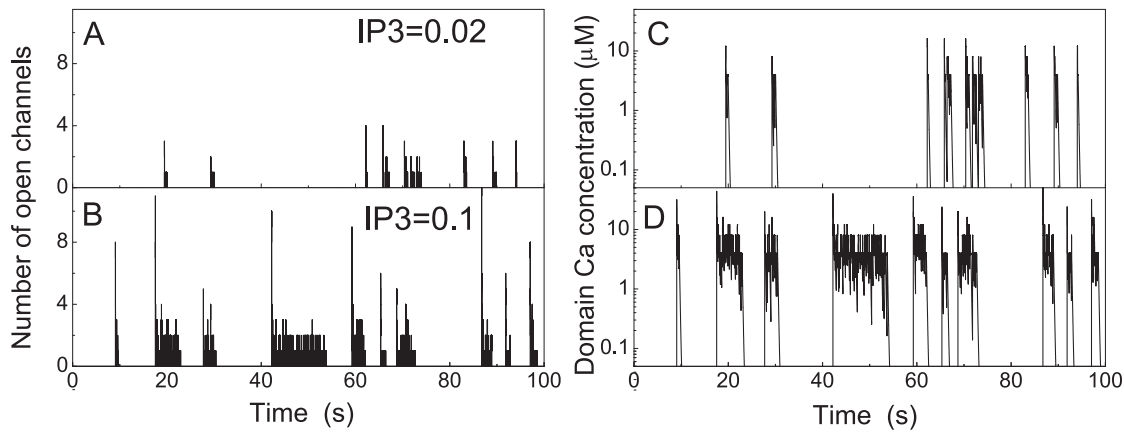


**Figure 5. Evolution of open channel number (A,B) and microdomain Ca<sup>2+</sup> concentration  $c$  (C,D) for clusters with 20 channels and decay rate  $r=10\text{ s}^{-1}$ .** A and C show traces for  $[\text{IP}_3]=0.02\text{ }\mu\text{M}$ , B and D for  $[\text{IP}_3]=0.1\text{ }\mu\text{M}$ . doi:10.1371/journal.pcbi.1002485.g005

event begins with the transition from 0 to 1 open channel and ends when the last channel closes, *i.e.*, when the number of channels is at zero again. However, to account for the noisy gating behavior sometimes observed in the wake of a release event, we consider the transition from 1 to 0 open channels not to be the end of the release event, if a re-opening of a channel occurs within a time span of 500 ms. The event is then considered terminated at the closing of the last channel if no further opening occurs within 500 ms. In Fig. 6 we characterize traces such as those in Fig. 5A,B accordingly for a range of values of  $[\text{IP}_3]$ . Here we have evaluated the typical lifetime of release events as well as the duration between consecutive events (interpuff interval, IPI). Fig. 6 shows that for  $r=10\text{ s}^{-1}$  both mean lifetime and mean interpuff interval generally increase with  $[\text{IP}_3]$ .

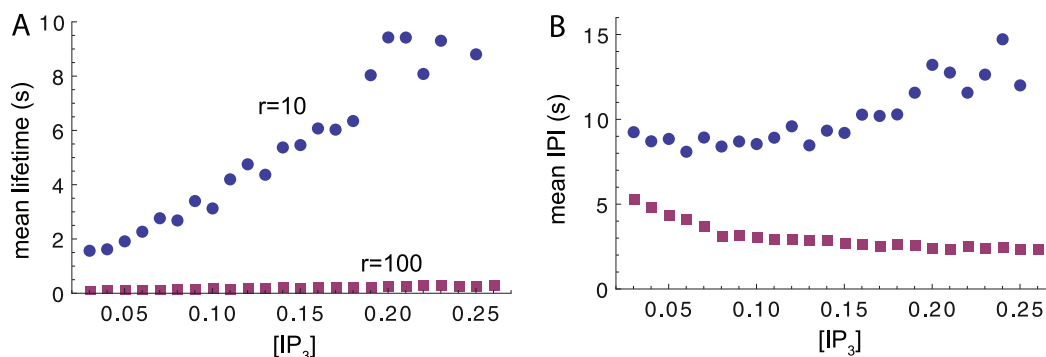
This result can be related to the transition from puffs to waves under increase of cytosolic IP<sub>3</sub> concentration. Within a stochastic theory of Ca<sup>2+</sup> release, wave generation can be understood in the following way. Waves begin by the random opening of one or a few clusters [36]. The released calcium spreads to neighboring clusters and because of their Ca<sup>2+</sup> dependent probability to open, the initial event triggers a wave. Increase of IP<sub>3</sub> supports the propagation of release activity since the duration and/or amplitude of the local trigger event increases and the excitability of neighboring clusters can increase. In this sense our result in Figs. 6A principally allows

to interpret the increase of lifetime as a transition from local to global release. When the  $[\text{IP}_3]$  parameter is increased, the duration of the cluster release prolongs. Therefore, for large  $[\text{IP}_3]$  cluster cooperativity is likely, while for small  $[\text{IP}_3]$  puffs are too short to allow propagation of activity. Here, however, we will not pursue this line of thought but instead focus on the effect of a change in decay rate  $r$ .

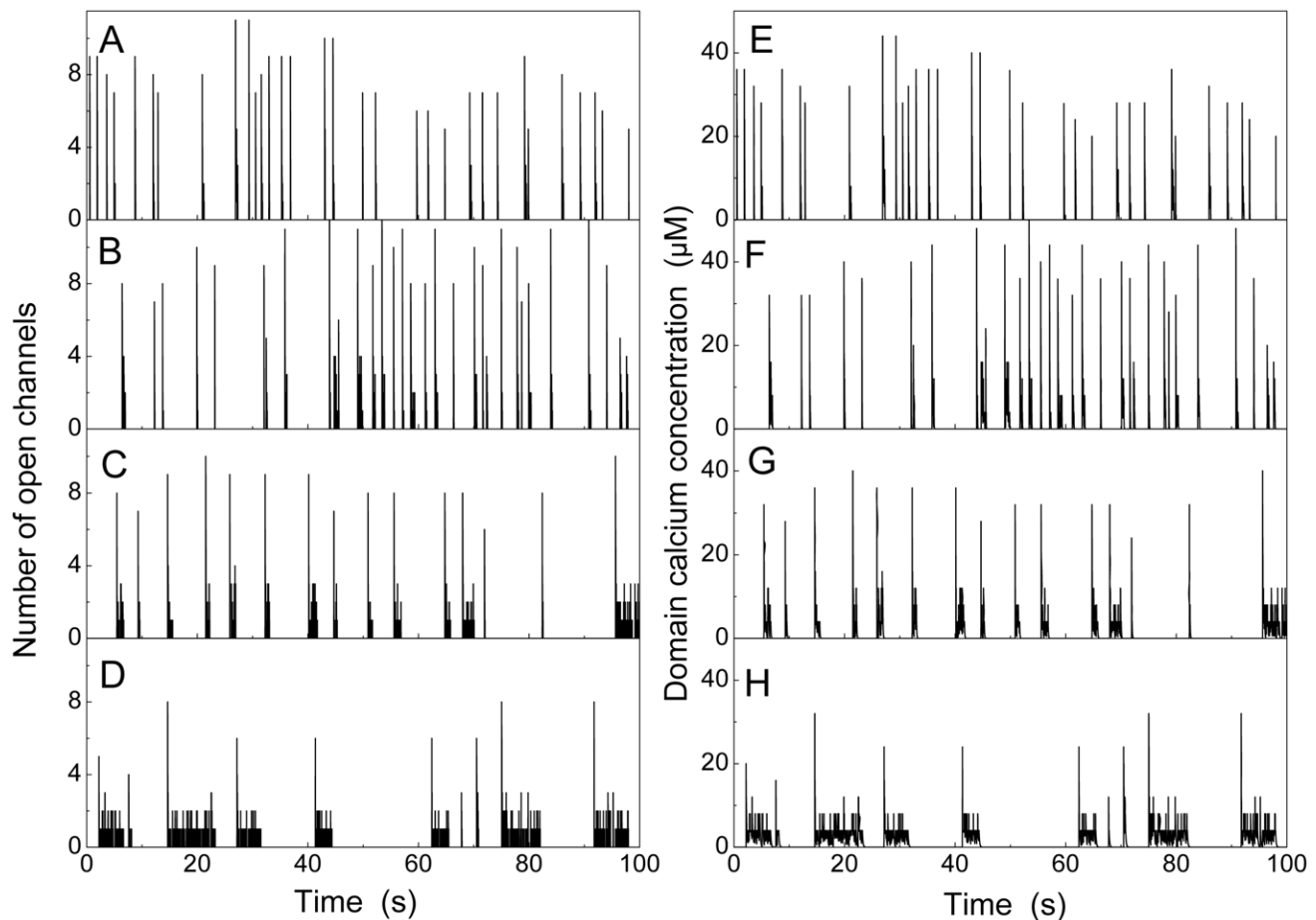
#### Dependence of release dynamics on decay rate

Fig. 6 also shows that the lifetime and IPI of release events strongly depends on the decay rate  $r$ . For large  $r=100\text{ s}^{-1}$  the mean lifetime is much smaller than for  $r=10\text{ s}^{-1}$ . We will now consider this dependence and its origin in detail. The IP<sub>3</sub> concentration will be set to  $p=0.07\text{ }\mu\text{M}$  in the following. This value is larger than  $d_1$ , so that in rest state the IP<sub>3</sub>R subunits are normally occupied by IP<sub>3</sub> and reside in the upper plane of the DYK cube (Fig. 2B).

Fig. 7 shows the typical evolution of open channel numbers for different values of the decay rate  $r$ . For large decay rate,  $r=100\text{ s}^{-1}$  we find frequent short spikes that resemble the experimentally observed puffs lasting less than 1 second. However, for smaller  $r$ , long events occur, which typically consist of one high initial spike and a burst of openings of decreasing amplitude (wave regime). Lifetime of wave-like release becomes increasingly longer as the decay rate decreases (Fig. 7).



**Figure 6. Dependence of mean lifetime (A) and mean interpuff interval (B) on the concentration of  $[\text{IP}_3]$  for two different values of decay rate  $r$ .**  $r=10\text{ s}^{-1}$  corresponds to long transients expected in absence of slow mobile buffer. Waves are experimentally found for large  $[\text{IP}_3]$  but not in the presence of slow mobile buffer. doi:10.1371/journal.pcbi.1002485.g006



**Figure 7. Evolution of open channel number (A–D) and microdomain Ca<sup>2+</sup> concentration  $c_d$  (E–H) for various decay rates  $r$ .** With decreasing  $r$  the trace shows longer and fewer events ( $r=100\text{ s}^{-1}$  (A,E),  $50\text{ s}^{-1}$  (B,F),  $20\text{ s}^{-1}$  (C,G),  $10\text{ s}^{-1}$  (D,H) at  $[\text{IP}_3]=0.07\text{ }\mu\text{M}$ ). doi:10.1371/journal.pcbi.1002485.g007

We will next analyze the behavior of channel gating that leads to the different dynamics of puffs and waves. Starting with the case of puffs (fast microdomain collapse), Fig. 8A shows the evolution of the number of open channels and Figs. 8B–D present the three quantities characterizing the inhibition and refractory behavior. Figs. 8B and C show the numbers of subunits in the particular inhibited states 111 and 011, respectively. The state 111 is obtained by direct transition from the open state, 110, while the local Ca<sup>2+</sup> is large. Fig. 8B clearly shows the fast onset of inhibition, which leads to the closing of all channels within about 200 ms. Because of the fast time scale of inhibition, not only is there a fast onset of inhibition, but, as seen in Fig. 8B, there is also only a short refractory time. The latter is caused by a fast rate of de-inhibition,  $b_2$ , which is around  $2\text{ s}^{-1}$ . This implies that the channels can be re-activated almost immediately after the termination of the last puff. However, because of the fast decay of Ca<sup>2+</sup> concentration for large  $r$ , calcium ions are normally too dilute to cause immediate re-openings.

We conclude that for (short) puffs the dynamics involves Ca<sup>2+</sup> activation and Ca<sup>2+</sup> inhibition of subunits. This result confirms earlier models of Ca<sup>2+</sup> dynamics, which relate the termination of Ca<sup>2+</sup> puffs to the binding of Ca<sup>2+</sup> to inhibiting binding site. This dynamics therefore does not need and does not incorporate the third component of the DYK model, which is the binding or unbinding of IP<sub>3</sub>. Fig. 8C shows that the number of subunits in state 011 (those subunits that have not bound IP<sub>3</sub> but have Ca<sup>2+</sup>

bound to the activating and inhibiting sites) does not change much during a puff. Fig. 8D shows the number of channels,  $U_{ip}$ , that have bound IP<sub>3</sub> to three or four subunits. Note that  $U_{ip}$  is the number of channels that are principally available for opening during a puff. Typically only a fraction of the 20 channels is available for opening (this effect will be discussed below.) Thus, Fig. 8D indicates no changes in IP<sub>3</sub> occupation during a puff. Taken together, our observations indicate that a typical trajectory of the subunits during puffs is a cycle that involves Ca<sup>2+</sup> activation and inhibition only. It thus only involves the upper horizontal plane of the DYK cube (see Fig. 9A).

We now discuss the behavior during the wave-like events occurring for smaller decay rate  $r$  (persistent Ca<sup>2+</sup> microdomains). Similarly to the case of short puffs, rapid inhibition occurs, which involves units transferring to the 111 state (Fig. 8F). However, because of the large transient microdomain [Ca<sup>2+</sup>], immediately after termination of an opening and restoration of subunits to the de-inhibited state, a further opening of channels occurs. This behavior leads to the perpetual cycling of some of the subunits around the upper plane of the DYK cube, explaining the occurrence of long bursts of openings shown in Fig. 8E.

One may think that the existence of longer signals for persistent Ca<sup>2+</sup> microdomains is simply a consequence of subunits cycling the activation/inhibition loop. However, we will now explain that the four states of the upper DYK cube are not sufficient to obtain the well-defined bursts shown in Fig. 8E. This relates to the fact



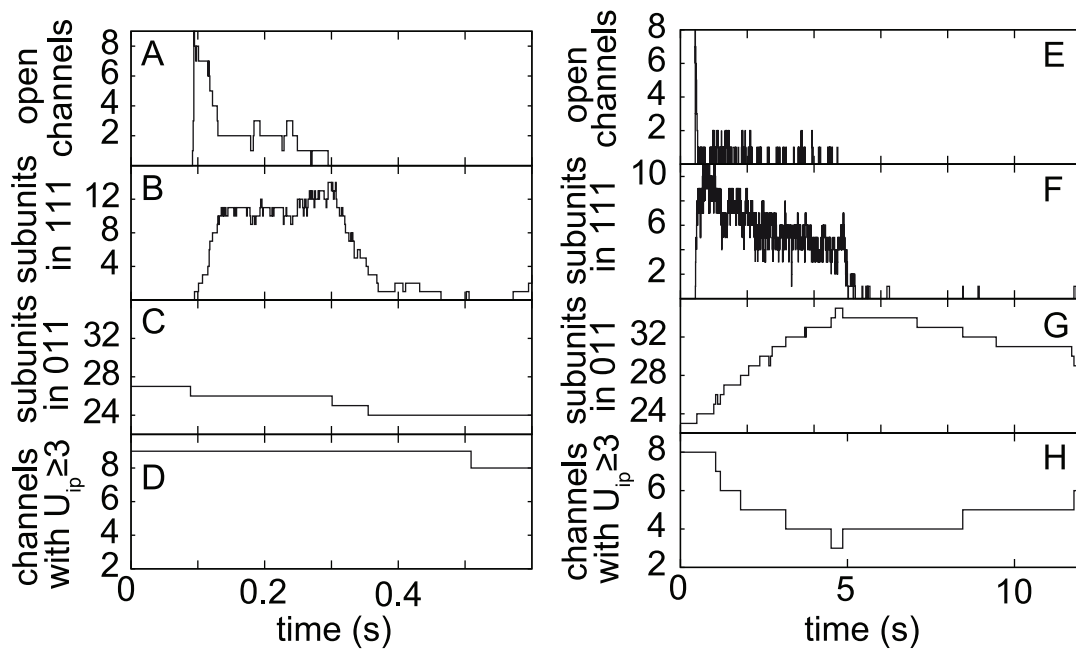


**Figure 8. Analysis of a single puff or burst for fast Ca<sup>2+</sup> decay,  $r=100\text{ s}^{-1}$  (left) and slow decay,  $r=10\text{ s}^{-1}$  (right).** Plots show the number of open channels (A,E), the number of subunits in the state 111 (B,F) and 011 (C,G) and the number of channels that have at least three subunits with IP<sub>3</sub> bound (D,H). Here  $U_{ip}$  denotes the number of subunits of a channel, which have IP<sub>3</sub> bound. doi:10.1371/journal.pcbi.1002485.g008

that subunits cycling along the upper loop need a further mechanism if they are to finally terminate the Ca<sup>2+</sup> release. Since inhibition is already part of the cycling that builds the bursts, another mechanism is needed to end the bursts. Surprisingly, our model suggests that the dissociation of IP<sub>3</sub> from subunits provides this mechanism.

First, Fig. 8G shows that during the course of a wave, more subunits accumulate in the state 011. The number of subunits in this state increases for this particular burst from 22 to 34, that is 12 subunits dissociate IP<sub>3</sub> during the burst. Note that the rates of IP<sub>3</sub> binding/unbinding are smaller than those of the other processes involved during a puff (see Supporting Text S1). Further, many of the channels have only three of the subunits bound to IP<sub>3</sub>, so that a further dissociated subunit means that the channel is not available for opening. Accordingly, the number of available channels drops from 8 to 3 during the burst event (Fig. 8H).

We found that the subunits undergo the IP<sub>3</sub> dissociation while being in the state 111. The mechanism of IP<sub>3</sub> dissociation therefore depends on the time that a subunit spends in the 111 state. This means that the IP<sub>3</sub> dissociation increases with the duration of Ca<sup>2+</sup> release. Fig. 9C shows that IP<sub>3</sub> dissociation indeed occurs for long release events. It thus constitutes a second inactivation process that is needed to terminate the wave-like release. Fig. 9B illustrates the mechanism, which involves gradual IP<sub>3</sub> dissociation of subunits while cycling the Ca<sup>2+</sup> activation/inhibition loop.

The IP<sub>3</sub> unbinding mechanism relies on the fact that the dissociation constants of IP<sub>3</sub> binding are very different for subunits with and without Ca<sup>2+</sup> bound to the inhibiting site. Stimulating levels of IP<sub>3</sub> concentration (*i.e.*, 0.07 μM in our simulations) are well above the value  $d_1$  (=0.001 μM), so that many subunits have bound IP<sub>3</sub>. However, inhibited subunits possess a much higher dissociation constant  $d_3$  (=0.7 μM), such that loss of IP<sub>3</sub> can occur while subunits populate the inhibited states. Therefore, the termination of waves due to IP<sub>3</sub> dissociation is possible only when

the IP<sub>3</sub> binding depends on inhibition. This leads to the conclusion that wave termination is related to the shift of peak open probability with IP<sub>3</sub> concentration (see Fig. 2B).

### Behavior of lifetime and interpuff interval and comparison to experiments

The effect described above lead to strong changes in the statistical properties of release events depending on the decay rate  $r$ . This concerns first of all the distribution of release lifetime. For fast collapse of the Ca<sup>2+</sup> microdomain, most events are of short duration. As an example, Fig. 10A shows the lifetime distribution for  $r=100\text{ s}^{-1}$  (dark gray bars). Most puffs in this case last between 100 and 300 ms. If, however, the  $r$  value is substantially lowered, most events last considerably longer than 1 s (light gray bars). Clearly, this behavior follows from the slow decay of microdomain Ca<sup>2+</sup> values and the related re-opening of channels.

Fig. 10B shows the dependence of average event lifetime on  $r$ . In the chosen range of  $r$  the event lifetime varies over one order of magnitude, which is what was observed in [12,31]. Our results resemble well the experimental findings for dependence of Ca<sup>2+</sup> release spikes if  $r$  is associated to the level of buffer concentration.

Interpuff intervals (IPI) have been experimentally determined as well. For puffs of small amplitude, Fraiman *et al.* found a distribution of IPIs peaked between 1 and 2 seconds and strongly decaying for larger intervals [37]. As can be seen in Fig. 10C, simulations of our model for  $r=100\text{ s}^{-1}$  yield a similar distribution with rare occurrence of IPIs with more than a few seconds (dark gray bars). If  $r$  is much smaller than this value, the distribution is much flatter. Correspondingly, the smaller the  $r$  the larger is the mean IPI (Fig. 10D).

The mean IPIs found in our simulations agree quantitatively with experimental values. In SH-SY5Y cells loaded with EGTA, puffs occur with a frequency of about 0.23 Hz, roughly corresponding to an IPI of four seconds [31]. In the absence of

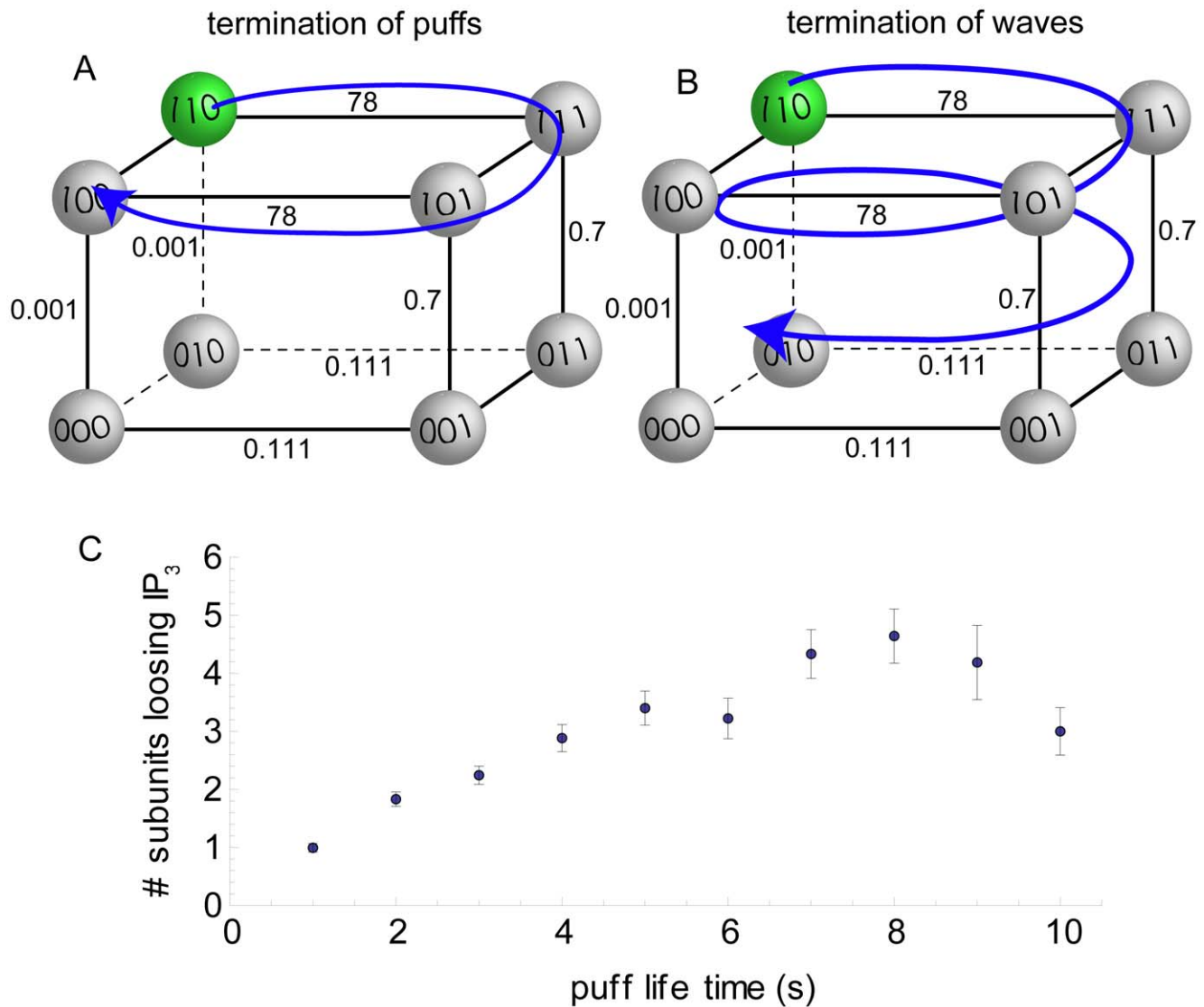


**Figure 9.** A and B illustrate the dynamics of subunits during a puffs (A) and burst (B). During short release (puff) only the upper plane of the DYK cube is populated by subunits of opening/closing channels (A). However, the more frequent the channels open, subunits in state 111 dissociate IP<sub>3</sub> and “cycle” down to the lower plane of the cube (B). Numbers show the dissociation constants of our model in μM. The loss of IP<sub>3</sub> occurs only for inhibited subunits, since only for inhibited subunits is [IP<sub>3</sub>] smaller than the dissociation constant ( $d_3 = 0.7 \mu\text{M}$ ). (C) shows the number of subunits that lose IP<sub>3</sub> during the course of a single puff or burst of puffs. For short puffs, few subunits dissociate IP<sub>3</sub>, while for long-lasting bursts up to 5 subunits lose IP<sub>3</sub>. The corresponding channels typically lose the ability to open. The data is taken from a single, long run with [IP<sub>3</sub>] = 0.07 μM and  $r = 10 \text{ s}^{-1}$ .

doi:10.1371/journal.pcbi.1002485.g009

EGTA, the experimental IPIs increase to about six seconds, again agreeing with our mean IPIs for small  $r = 10 \text{ s}^{-1}$ . These numbers demonstrate the realistic representation of experimental results in [31] by our modeling approach.

In view of the mechanism proposed in this paper, the increase of IPI for small  $r$  appears to be counter-intuitive. If residual Ca<sup>2+</sup> is large, one would naively expect that a higher activation probability and thus an earlier appearance of the next wave results. Therefore, for small  $r$  one could expect shorter IPIs. Here, however, we find for small  $r$  that the next wave occurs typically several seconds later. In fact, this delay is not the result of simply a longer lifetime of release events. Figs. 10E,F present the time of dormancy between two consecutive release events, *i.e.*, the length of intervals in which no channel is open. The increase of dormancy interval for

persistent residual microdomains (small  $r$ ) indicates the presence of a refractory mechanism that suppresses the probability of wave generation for a few seconds. We briefly would like to discuss the origin of this behavior.

We first remind that for large  $r$  a very short refractory period after the termination of a puff was noticed (see Fig. 8B). The refractory period is the time where channels are inhibited or otherwise not available for re-opening. This time is of the order of at most a few hundreds ms. This means that the refractory period cannot account for the mean IPI for large  $r$ , which is at around 4 s. Instead, most of the IPI for large  $r$  is related to a waiting time for a first “trigger” channel to open [38].

The small  $r$  case, however, provides a different scenario. Clearly, the large number of IP<sub>3</sub> unbinding subunits decreases the

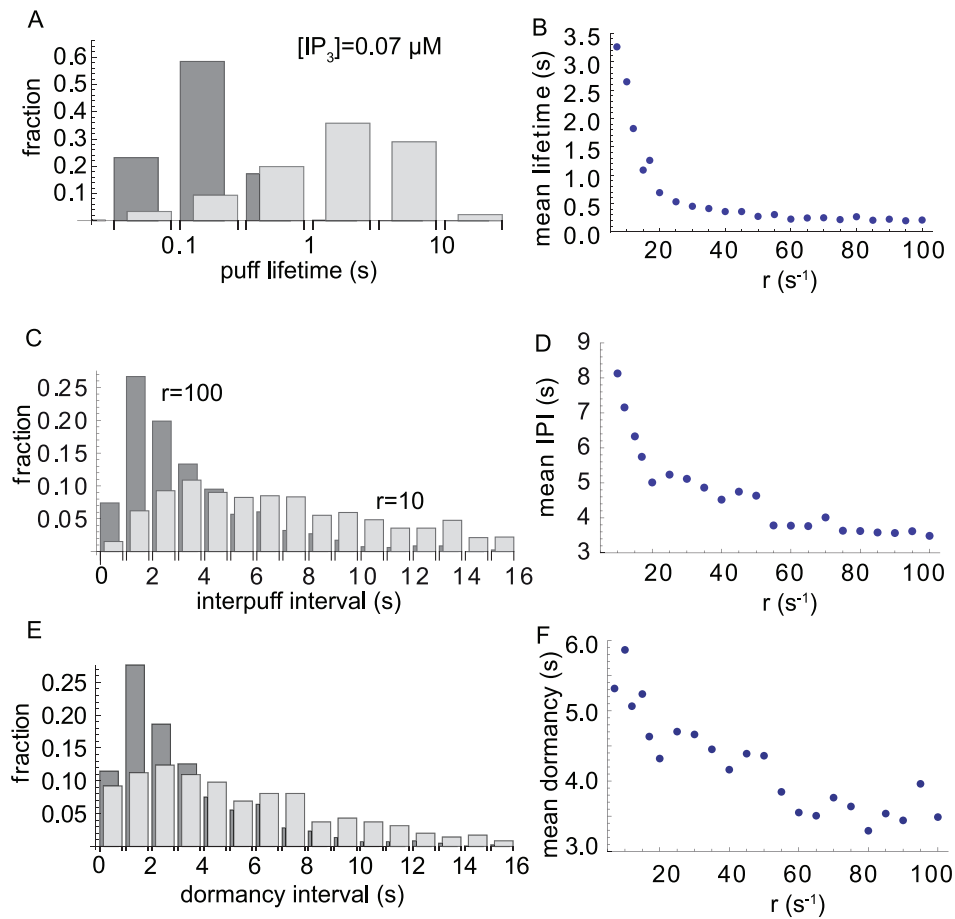


**Figure 10.** (A) Lifetime distribution for  $r = 10$  s<sup>-1</sup> (light gray) and  $r = 100$  s<sup>-1</sup> (dark gray). (B) The mean life time decreases with increasing decay rate  $r$ . (C) IPI distribution for  $r = 10$  s<sup>-1</sup> and  $r = 100$  s<sup>-1</sup>. (D) The mean interpuff interval decreases with increasing decay rate  $r$ . (E) and (F) show the dormancy interval, *i.e.*, the time between puffs, during which no channel is open. (All data for  $p = 0.07$  μM.)  
doi:10.1371/journal.pcbi.1002485.g010

probability of re-opening. The loss of IP<sub>3</sub> thus amounts to a kind of refractory period. The chance of triggering a wave is much smaller after long-lasting events where many IP<sub>3</sub> molecules are lost (Fig. 9C), mainly because the number of channels available for opening is smaller. Only after this refractory period, channels have re-bound the lost IP<sub>3</sub> and regain their potential to trigger a wave. It is interesting to note that this IP<sub>3</sub> refractoriness should generally reduce Ca<sup>2+</sup> excitability. It may therefore provide a new mechanistic explanation for the smaller excitability of cells for the first few seconds after waves [36].

## Discussion

The spatio-temporal patterns of Ca<sup>2+</sup> signals are known to depend on many factors, including the IP<sub>3</sub> concentration and the presence of buffer proteins. We have here discussed the role of “hidden” quantities in the shaping of Ca<sup>2+</sup> signals and argued that they may serve as mediators of signal modulation. We have shown that their dynamics can explain features of Ca<sup>2+</sup> puffs and waves in a consistent way.

Most importantly, our analysis reveals that changes in the collapse of Ca<sup>2+</sup> microdomains can have a profound effect on release duration. In this paper, we have represented this collapse of Ca<sup>2+</sup> microdomain by the rate  $r$ , which describes the decay of residual Ca<sup>2+</sup> in the microdomain after closing of channels. The most significant result is that for slow collapse (small  $r$ ) one

generally finds long release reminiscent to temporal evolution during global waves, while for fast collapse much shorter events – puffs – appear. For slow collapse, residual free Ca<sup>2+</sup> re-activates channels by binding to their activating binding sites soon after channel closing. Often, re-activation leads to re-opening of channels because the refractory time of open channels is relatively short, *i.e.*, inhibited subunits unbind Ca<sup>2+</sup> from their inhibited sites shortly after the channel has closed and are therefore available for re-opening. This property distinguishes the IP<sub>3</sub> - Ca<sup>2+</sup> system from other excitable systems where refractoriness lasts much longer than the actual spike [39].

## Termination of puffs and waves

Since the durations of puffs and waves are so different, it is natural to expect that there should be different processes responsible for the termination of release. Many experimental and modeling studies have proposed that puffs are terminated by Ca<sup>2+</sup> -inhibition. Our earlier results [17] and the analysis presented here also support the idea that puffs are terminated by Ca<sup>2+</sup> binding to inhibiting sites. An unexpected outcome of our work is that for “long puffs” (or waves) termination occurs largely by way of IP<sub>3</sub> -unbinding. This effect is based on the dependence of Ca<sup>2+</sup> dissociation constants on IP<sub>3</sub>. The special form of the dependence, as well as the related shift in the peak location of open probability, is an often neglected trait of IP<sub>3</sub> receptor gating. Ca<sup>2+</sup>

inhibition and IP<sub>3</sub> dissociation thus present dual mechanisms that not only provide a surprising answer to the long-standing puzzle of release termination, but also assign a function to the control of Ca<sup>2+</sup> inhibition by IP<sub>3</sub>. Our results highlight the meaning of complex IP<sub>3</sub>R gating models such as the DYK model and require that future studies need not oversimplify IP<sub>3</sub>R gating schemes.

### Buffers and the puff-wave transition

The effect that we describe provides a novel explanation of the action of EGTA buffer on Ca<sup>2+</sup> release. Experiments with various exogenous buffers have clearly demonstrated the strong effect of buffers on dynamics of Ca<sup>2+</sup> release [12,40]. Dargan et al. [12,41] studied how the Ca<sup>2+</sup> signal depends on buffers injected into *Xenopus* oocytes. In these experiments, the amount of Ca<sup>2+</sup> in the cytosol after stimulation by IP<sub>3</sub> was measured by fluorescence recordings using an additional dye buffer. For EGTA buffer the response to the IP<sub>3</sub> stimulation was sharply shortened compared to the release in untreated cells. In contrast, BAPTA-injection leads to a more homogeneous and prolonged release.

By relating large values of  $r$  with the action of EGTA on calcium domains our results imply a shortening effect of EGTA on release of calcium. It is important to note that the release duration here refers to the proper open state of channels in a cluster and not to indirect effects due to a dye-buffer competition, which may additionally shorten traces of puffs in cells loaded with EGTA [12,42]. To our knowledge, our work is the first theoretical study to show the consequences of EGTA and similar slow buffers on channel gating dynamics within a cluster.

How realistic is our assumption that the presence of EGTA speeds up the collapse of Ca<sup>2+</sup> microdomains? Earlier work on full reaction-diffusion equations for buffer and Ca<sup>2+</sup> has shown that the collapse of free Ca<sup>2+</sup> concentration at the channel pore after closing of the channel strongly depends on the mobile buffer present in the system [20]. Our detailed three-dimensional simulations have shown, for instance, that in the presence of EGTA a free Ca<sup>2+</sup> concentration of 0.5 μM is reached after less than 1 ms, while in the absence of EGTA it takes about 6 ms. This observation serves as motivation for the simplified decay dynamics for free Ca<sup>2+</sup> concentration in our model.

Having argued that the effect of EGTA is to accelerate the collapse of Ca<sup>2+</sup> microdomain, it remains to discuss why, experimentally, the presence of BAPTA does not lead to puffs and shortening of release. The difference between the cases of EGTA and BAPTA can be attributed to the different kinetic rates of Ca<sup>2+</sup> binding/unbinding. EGTA is a buffer that binds Ca<sup>2+</sup> relatively slow, while BAPTA reacts around 100 times faster. This

implies that BAPTA can interrupt the communication between channels during a puff [20], while EGTA is too slow to bind substantial amounts of Ca<sup>2+</sup> during a puff. In other words, BAPTA reduces the peak levels of microdomain [Ca<sup>2+</sup>] in Fig. 1 and residual [Ca<sup>2+</sup>], while EGTA only diminishes residual [Ca<sup>2+</sup>]. We therefore speculate that the fast intra-cluster action of BAPTA leads to a very different dynamics, for instance by reducing the initial phase of a puff or reducing inhibition. Detailed analysis of this problem will be performed in the future.

With respect to physiological conditions *in vivo*, our results suggest that the duration of IP<sub>3</sub>-evoked Ca<sup>2+</sup> signals is a highly variable quantity. Experimentally the lifetime depends not only on IP<sub>3</sub> concentration and buffer content but was also shown to be sensitive for instance to changes in temperature [43]. The mobile buffer, however, appears to be special in that it allows control not only of the duration of release events but also of channel cooperativity. The concentration of cell specific buffer such as the Ca<sup>2+</sup> binding protein parvalbumin is one example showing the importance for tuning the duration of local IP<sub>3</sub>-evoked Ca<sup>2+</sup> signals. Parvalbumin is a slow Ca<sup>2+</sup> binding protein, which is known to have an important physiological role in muscle and neuronal cells. John *et al.* have shown that parvalbumin, similar to EGTA, inhibits repetitive Ca<sup>2+</sup> waves and evokes release at discrete release sites [22]. Buffer concentration determines the sensitivity and cooperativity of IP<sub>3</sub> action and confers a threshold for the ability of the cell to transition from a local to a global mode of Ca<sup>2+</sup> signaling. It is therefore possible that cell-specific expression of parvalbumin and potentially other buffers may serve to shape intracellular Ca<sup>2+</sup> puff and wave signals for specific physiological roles by the mechanism described in this paper.

### Supporting Information

**Text S1** Method and results of the single channel data fitting. (PDF)

**Text S2** Description of stochastic simulation method. (PDF)

### Acknowledgments

We would like to acknowledge many useful conversations with Ian Parker.

### Author Contributions

Analyzed the data: SR PJ JWS. Wrote the paper: SR PJ JWS. Conceived model: SR JWS Wrote computer code: SR JWS.

### References

- Berridge M, Lipp P, Bootman M (2000) The versatility and universality of calcium signalling. *Nat Rev Mol Cell Biol* 1: 11–22.
- Berridge M, Bootman M, Roderick H (2003) Calcium signalling: dynamics, homeostasis and remodelling. *Nat Rev Mol Cell Biol* 4: 517–529.
- Foskett J, White C, Cheung K, Mak D (2007) Inositol Trisphosphate Receptor Ca<sup>2+</sup> Release Channels. *Physiol Rev* 87: 593.
- Dupont G, Combettes L, Leybaert L (2007) Calcium dynamics: spatiotemporal organization from the subcellular to the organ level. *Int Rev Cyt* 261: 193–245.
- Smith I, Parker I (2009) Imaging the quantal substructure of single IP<sub>3</sub>R channel activity during Ca<sup>2+</sup> puffs in intact mammalian cells. *Proc Natl Acad Sci U S A* 106: 6404.
- Wei C, Wang X, Chen M, Ouyang K, Song L, et al. (2008) Calcium ickers steer cell migration. *Nature* 457: 901–905.
- Di Capite J, Ng S, Parekh A (2009) Decoding of cytoplasmic Ca<sup>2+</sup> oscillations through the spatial signature drives gene expression. *Curr Biol* 19: 853–858.
- Parekh A (2010) Decoding cytosolic ca<sup>2+</sup> oscillations. *Trends Biochem Sci* 36: 78.
- Berridge M (1990) Calcium oscillations. *J Biol Chem* 265: 9583–9586.
- Rooney T, Sass E, Thomas A (1989) Characterization of cytosolic calcium oscillations induced by phenylephrine and vasopressin in single fura-2-loaded hepatocytes. *J Biol Chem* 264: 17131–17141.
- Lechleiter J, Girard S, Peralta E, Clapham D (1991) Spiral calcium wave propagation and annihilation in *Xenopus laevis* oocytes. *Science* 252: 123–126.
- Dargan S, Parker I (2003) Buffer kinetics shape the spatiotemporal patterns of IP<sub>3</sub>-evoked Ca<sup>2+</sup> signals. *J Physiol* 553: 775–788.
- Swillens S, Dupont G, Champeil P (1999) From calcium blips to calcium puffs: Theoretical analysis of the requirements for interchannel communication. *Proc Natl Acad Sci U S A* 96: 13750–13755.
- Shuai J, Jung P (2003) Optimal ion channel clustering for intracellular calcium signaling. *Proc Natl Acad Sci U S A* 100: 506–510.
- DeRemigio H, Groff J, Smith G (2008) Calcium release site ultrastructure and the dynamics of puffs and sparks. *Math Med Biol* 25: 65.
- Swaminathan D, Ullah G, Jung P (2009) A simple sequential-binding model for calcium puffs. *Chaos* 19: 037109.
- Rüdiger S, Shuai J, Sokolov I (2010) Law of mass action, detailed balance, and the modeling of calcium puffs. *Phys Rev Lett* 105: 048103.

18. Bruno L, Solovey G, Ventura A, Dargan S, Dawson S (2010) Quantifying calcium uxes underlying calcium puffs in xenopus laevis oocytes. *Cell Calcium* 47: 273–286.
19. Thurlley K, Smith I, Tovey S, Taylor C, Parker I, et al. (2011) Timescales of ip3-evoked ca2+ spikes emerge from ca2+ puffs only at the cellular level. *Biophys J* 101: 2638–2644.
20. Rüdiger S, Nagaiah C, Warnecke G, Shuai J (2010) Calcium Domains around Single and Clustered IP3 Receptors and Their Modulation by Buffers. *Biophys J* 99: 3–12.
21. Neher E, Augustine G (1992) Calcium gradients and buffers in bovine chromaffin cells. *J Physiol* 450: 273–301.
22. John L, Mosquera-Caro M, Camacho P, Lechleiter J (2001) Control of IP3-mediated Ca<sup>2+</sup> puffs in xenopus laevis oocytes by the Ca<sup>2+</sup>-binding protein parvalbumin. *J Physiol* 535: 3.
23. Taylor C, Tovey S (2010) IP<sub>3</sub> receptors: Toward understanding their activation. *Cold Spring Harb Perspect Biol* 2: a004010.
24. DeYoung G, Keizer J (1992) A single-pool inositol 1,4,5-trisphosphate-receptor-based model for agonist-stimulated oscillations in Ca<sup>2+</sup> concentration. *Proc Natl Acad Sci U S A* 89: 9895–9899.
25. Sneyd J, Dufour J (2002) A dynamic model of the type-2 inositol trisphosphate receptor. *Proc Natl Acad Sci U S A* 99: 2398.
26. Watras J, Bezprozvanny I, Ehrlich B (1991) Inositol 1,4,5-trisphosphate-gated channels in cerebellum: presence of multiple conductance states. *J Neurosci* 11: 3239–3245.
27. Shuai J, Yang D, Pearson J, Rüdiger S (2009) An investigation of models of the IPR channel in Xenopus oocyte. *Chaos* 19: 037105.
28. Mak D, Foskett J (1997) Single-channel kinetics, inactivation, and spatial distribution of inositol trisphosphate (IP3) receptor in Xenopus oocyte nucleus. *J Gen Physiol* 109: 571–587.
29. Mak D, McBride S, Foskett J (1998) Inositol 1,4,5-tris-phosphate activation of inositol trisphosphate receptor Ca<sup>2+</sup> channel by ligand tuning of Ca<sup>2+</sup> inhibition. *Proc Natl Acad Sci U S A* 95: 15821–15825.
30. Demuro A, Parker I (2008) Multi-dimensional resolution of elementary Ca<sup>2+</sup> signals by simultaneous multi-focal imaging. *Cell Calcium* 43: 367–374.
31. Smith I, Wiltgen S, Parker I (2009) Localization of puff sites adjacent to the plasma membrane: Functional and spatial characterization of Ca2+ signaling in SH-SY5Y cells utilizing membranepereant caged IP3. *Cell Calcium* 45: 65–76.
32. Thul R, Falcke M (2004) Release currents of IP3 receptor channel clusters and concentration profiles. *Biophys J* 86: 2660–2673.
33. Shuai J, Pearson J, Parker I (2008) Modeling Ca<sup>2+</sup> Feedback on a Single Inositol 1, 4, 5-Trisphosphate Receptor and Its Modulation by Ca<sup>2+</sup> Buffers. *Biophys J* 95: 3738.
34. Mazzag B, Tiganelli C, Smith G (2005) The effect of residual Ca<sup>2+</sup> on the stochastic gating of Ca<sup>2+</sup>-regulated Ca<sup>2+</sup> channel models. *J Theor Biol* 235: 121–150.
35. Tanimura A, Morita T, Nezu A, Shitara A, Hashimoto N, et al. (2009) Use of uorescence resonance energy transfer-based biosensors for the quantitative analysis of inositol 1, 4, 5-trisphosphate dynamics in calcium oscillations. *J Biol Chem* 284: 8910.
36. Marchant J, Callamaras N, Parker I (1999) Initiation of IP3-mediated Ca<sup>2+</sup> waves in Xenopus oocytes. *EMBO J* 18: 5285–5299.
37. Fraiman D, Pando B, Dargan S, Parker I, Dawson S (2006) Analysis of puff dynamics in oocytes: interdependence of puff amplitude and interpuff interval. *Biophys J* 90: 3897–3907.
38. Thul R, Falcke M (2006) Frequency of elemental events of intracellular Ca<sup>2+</sup> dynamics. *Phys Rev E* 73: 61923.
39. Izhikevich E (2007) Dynamical systems in neuroscience: the geometry of excitability and bursting. The MIT press. 441 p.
40. Rintoul G, Baimbridge K (2003) Effects of calcium buffers and calbindin-D28k upon histamineinduced calcium oscillations and calcium waves in HeLa cells. *Cell Calcium* 34: 131–144.
41. Dargan S, Schwaller B, Parker I (2004) Spatiotemporal patterning of IP3-mediated Ca<sup>2+</sup> signals in Xenopus oocytes by Ca<sup>2+</sup>-binding proteins. *J Physiol* 556: 447–461.
42. Zeller S, Rüdiger S, Engel H, Sneyd J, Warnecke G, et al. (2009) Modeling of the Modulation by Buffers of Ca2+ Release through Clusters of IP3 Receptors. *Biophys J* 97: 992–1002.
43. Schipke C, Heidemann A, Skupin A, Peters O, Falcke M, et al. (2008) Temperature and nitric oxide control spontaneous calcium transients in astrocytes. *Cell Calcium* 43: 285–295.